ELSEVIER

International Journal of Solids and Structures 41 (2004) 1473–1489

INTERNATIONAL JOURNAL OF SOLIDS and STRUCTURES

www.elsevier.com/locate/ijsolstr

Mixed mode BEM analysis of multiple curvilinear cracks in the general anisotropic solids by the crack tip singular element

M. Denda [a,*], M.E. Marante [b,c]

[a] Department of Mechanical and Aerospace Engineering, Rutgers University, 98 Brett Road, Piscataway, NJ 08854-8058, USA
[b] Department of Structural Engineering, Lisandro Alvarado University, Barquisimeto, Venezuela
[c] Department of Structural Engineering, University of Los Andes, Mérida 5101, Venezuela

Received 23 April 2003

Abstract

We consider multiple curvilinear cracks in the two-dimensional general anisotropic solids and establish a computationally effective technique to determine the stress intensity factors accurately. Each curvilinear crack is represented by a collection of straight crack elements and the crack opening displacement (COD) by the continuous distribution of the dislocation dipoles. The crack element located next to the crack tip is called the crack tip singular element (CTSE), where the known $\sqrt{r}$ crack tip opening displacement and the $1/\sqrt{r}$ stress singularity is mathematically built in the interpolation of the COD using the Chebyshev polynomials. The regular crack elements away from the crack tip use the quadratic polynomial interpolation for the CODs.

Simple analytical formulas for the displacement, traction, and the stress intensity factor (SIF) contributions for the CTSE are developed in terms of its own COD coefficients. Since the SIFs are obtained during the main processing no post processing is required; a distinct advantage over the powerful quarter-point element. Numerical results are given for several multiple curvilinear crack problems to demonstrate the accuracy and simplicity of the technique.

Keywords: Boundary element method; Singular crack tip element; Generalized plane strain anisotropic elasticity; Mixed mode multiple crack analysis

1. Introduction

We will develop the boundary element method for the mixed mode fracture analysis of multiple curvilinear cracks in the general anisotropic solids in two dimensions. Under the assumption of the generalized plane strain three modes, in-plane Mode I, II, and out-of-plane Mode III, of fracture could be coupled. Such a coupling is found in the fracture analysis of the triclinic, monoclinic and trigonal crystal systems. The other crystals which have a plane of symmetry normal to the x_3-axis (i.e., the out-of-plane axis) also exhibit this coupling when their crystal axes are rotated out of the symmetry position.

* Corresponding author. Tel.: +1-732-445-4391; fax: +1-732-445-3124.
E-mail address: denda@jove.rutgers.edu (M. Denda).

0020-7683/$ - see front matter © 2003 Elsevier B.V. All rights reserved.
doi:10.1016/j.ijsolstr.2003.11.005

The majority of the existing BEM for the two-dimensional fracture analysis for the anisotropic solids have dealt with the decoupled cases of the plane strain and stress (Snyder and Cruse, 1975; Sollero and Aliabadi, 1993; Denda, 1999). The coverage of the generalized plane strain in the fracture analysis is limited (Ang and Clements, 1986; Berger and Tewary, 1997; Tan et al., 1992; Denda, 2001; Denda and Mattingly, 2003). With the exception of Denda (2001) and Denda and Mattingly (2003), who have addressed the full coupling of the three modes, all others dealt with simpler decoupled cases in the generalized plane strain.

In modeling of the crack tip singularity in anisotropic solids Snyder and Cruse (1975) used the Green's function for the single crack which calculated the stress intensity factors analytically without modeling the crack surface. Tan and Gao (1992) used the quarter-point traction and displacement crack tip elements from which the analytical expressions for the stress intensity factors were derived. The dual boundary element method of Sollero and Aliabadi (1993) used the J-integral and the dislocation dipole approach of Denda (1999, 2001) adopted the conservation integral developed by Chen and Shield (1977) to calculate SIFs, respectively. Despite an excellent accuracy of the SIF results by the conservation integrals, the post-processing requirement is an extra burden for the multiple cracks problems. The Green's function approach does not require the post-processing since it uses the analytic expression for the SIF; however, the method is limited to single straight crack problems. In extending the dislocation dipole approach of Denda (1999, 2001), Denda and Mattingly (2003) interpolated the crack opening displacement (COD) of a single straight crack with the product of the $\sqrt{a^2 - X^2}$ weight function and Chebyshev polynomials and obtained the analytical SIF formula in terms of the COD coefficients of the polynomials, where X is the local crack coordinate along the crack of half length a. This crack element is called the whole crack singular element (WCSE). Since the analytical formula gives the SIFs as an integral part of the solution the post-processing is not required. The corresponding WCSE for the isotropic solids was developed by Denda and Dong (1997). Although the WCSE can handle multiple straight center cracks effectively, it has no capability for the edge and curvilinear cracks. For isotropic solids, Denda and Dong (1999) proposed the crack tip singular element (CTSE), which is a small WCSE element embedded at each crack tip, to extend the capability of the WCSE to multiple curvilinear cracks.

The objective of this paper is to develop the crack tip singular element for the general anisotropic solids in 2-D. The CTSE is placed locally at each crack tip on top of the ordinary non-singular crack elements that cover the entire crack surface. Any curvilinear cracks, including center and edge cracks, can be modelled rectilinearly. Since the quarter-point element does not provide an analytical formula for the stress intensity factor, an indirect procedure, such as the J-integral, must be used to calculate the stress intensity factor. The CTSE overcomes this disadvantage of the quarter-point element by providing the SIF as an integral part of the main solution. It is an ideal fracture analysis tool for 2-D multiple curvilinear cracks in the general anisotropic solids.

2. Stroh formalism for 2-D general anisotropic solids

We consider the generalized plane strain problem where the displacement components u_i $(i = 1, 2, 3)$ depend only on two coordinates x_1 and x_2. Replace the pair of suffices by the single suffix according to $(11 \to 1)$, $(22 \to 2)$, $(33 \to 3)$, $(23 \to 4)$, $(31 \to 5)$, $(12 \to 6)$ for the stress, strain and compliance components. The non-zero stain components are given by

$$e_1 = \frac{\partial u_1}{\partial x_1}, \quad e_2 = \frac{\partial u_2}{\partial x_2}, \quad e_4 = \frac{\partial u_3}{\partial x_2}, \quad e_5 = \frac{\partial u_3}{\partial x_1}, \quad e_6 = \frac{\partial u_2}{\partial x_1} + \frac{\partial u_1}{\partial x_2} \tag{1}$$

and the strain–stress relations by

$$e_M = \sum_{N=1}^{6} S_{MN}\sigma_N \quad (M,N = 1,2,4,5,6), \tag{2}$$

where S_{MN} is the reduced compliance defined by

$$S_{MN} = s_{MN} - (s_{M3}s_{3N})/s_{33} \quad (M,N = 1,2,4,5,6) \tag{3}$$

in terms of the 3-D compliance constants s_{MN} $(M,N = 1,2,3,4,5,6)$. In this paper, the summation over an index is indicated explicitly without using the summation convention for the repeated indices.

The displacement u_i and the stress function ϕ_i are given in the form (Lekhnitskii, 1963; Eshelby et al., 1953)

$$u_i = 2\Re\sum_{\alpha=1}^{3} A_{i\alpha}f_\alpha(z_\alpha), \quad \phi_i = 2\Re\sum_{\alpha=1}^{3} L_{i\alpha}f_\alpha(z_\alpha) \tag{4}$$

in terms of three analytic functions $f_1(z_1)$, $f_2(z_2)$ and $f_3(z_3)$ of the generalized complex variables $z_\alpha = x_1 + p_\alpha x_2$ for $\alpha = 1,2,3$. Here p_α, along with their conjugates, are the three distinct roots of the sixth-order polynomial characteristic equation

$$d^{(4)}(p)d^{(2)}(p) - d^{(3)}(p)d^{(3)}(p) = 0, \tag{5}$$

where

$$d^{(4)}(p) = p^4S_{11} - 2p^3S_{16} + p^2(2S_{12} + S_{66}) - 2pS_{26} + S_{22},$$

$$d^{(3)}(p) = p^3S_{15} - p^2(S_{14} + S_{56}) + p(S_{25} + S_{46}) - S_{24},$$

$$d^{(2)}(p) = p^2S_{55} - 2pS_{45} + S_{44}.$$

The coefficients $L_{i\alpha}$ in (4) are given, as the the components of 3×3 matrix $\mathbf{L}$, by

$$\mathbf{L} = [L_{i\alpha}] = \begin{bmatrix} -p_1L_{21} & -p_2L_{22} & -p_3r_3L_{33} \\ L_{21} & L_{22} & r_3L_{33} \\ r_1L_{21} & r_2L_{22} & L_{33} \end{bmatrix}, \tag{6}$$

where

$$r_1 = \frac{d^{(3)}(p_1)}{d^{(2)}(p_1)}, \quad r_2 = \frac{d^{(3)}(p_2)}{d^{(2)}(p_2)}, \quad r_3 = \frac{d^{(3)}(p_3)}{d^{(4)}(p_3)}. \tag{7}$$

Let $\mathbf{l}_\alpha = \{L_{1\alpha}, L_{2\alpha}, L_{3\alpha}\}^{\mathrm{T}}$ represent αth column of the matrix $\mathbf{L}$. The coefficients $A_{i\alpha}$ in (4) are given as the components of the 3×3 matrix $\mathbf{A}$ defined by

$$\mathbf{A} = [\mathbf{a_1}, \mathbf{a_2}, \mathbf{a_3}], \tag{8}$$

where

$$\mathbf{a}_\alpha = \begin{Bmatrix} A_{1\alpha} \\ A_{2\alpha} \\ A_{3\alpha} \end{Bmatrix} = \begin{bmatrix} s_{16} - s_{11}p_\alpha, & s_{12}, & s_{14} - s_{15}p_\alpha \\ \dfrac{s_{26} - s_{21}p_\alpha}{p_\alpha}, & \dfrac{s_{22}}{p_\alpha}, & \dfrac{s_{24} - s_{25}p_\alpha}{p_\alpha} \\ s_{56} - s_{51}p_\alpha, & s_{52}, & s_{54} - s_{55}p_\alpha \end{bmatrix} \begin{Bmatrix} L_{1\alpha} \\ L_{2\alpha} \\ L_{3\alpha} \end{Bmatrix} \quad (\alpha = 1,2,3). \tag{9}$$

Note that for each characteristic root p_α we determine vectors $\mathbf{l}_\alpha = \{L_{1\alpha}, L_{2\alpha}, L_{3\alpha}\}^{\mathrm{T}}$ and $\mathbf{a}_\alpha = \{A_{1\alpha}, A_{2\alpha}, A_{3\alpha}\}^{\mathrm{T}}$ up to an arbitrary multiplying factor, which can be normalized by (Denda, 2001) the relation

$$2\sum_{i=1}^{3} L_{i\alpha}A_{i\alpha} = 1 \quad (\alpha = 1,2,3). \tag{10}$$

The stress components σ_{ij} are given by

$$\sigma_{1i} = -\frac{\partial \phi_i}{\partial x_2}, \quad \sigma_{2i} = \frac{\partial \phi_i}{\partial x_1}. \tag{11}$$

3. Direct formulation of the BEM

Consider a finite domain R bounded by the contour ∂R where the displacement u_j and the traction t_j are applied. We adopt the physical interpretation of Somigliana's identity (Denda, 2001; Altiero and Gavazza, 1980; Eshelby, 1969) to formulate the direct BEM in terms of the distributions of line forces t_j and dislocation dipoles u_j, respectively, over ∂R embedded in the infinite domain. The two fundamental solutions, the line force and the dislocation dipole, are obtained using the Stroh formalism outlined in the previous section. A line force in x_k direction at (η_1, η_2) gives rise to the displacement component in the x_j direction at (x_1, x_2)

$$G_{jk}(x_1, x_2; \eta_1, \eta_2) = \Im \frac{1}{\pi} \sum_{\alpha=1}^{3} A_{j\alpha}A_{k\alpha} \ln(z_\alpha - \xi_\alpha), \tag{12}$$

where $z_\alpha = x_1 + p_\alpha x_2$ and $\xi_\alpha = \eta_1 + p_\alpha \eta_2$ ($\alpha = 1,2,3$) and $\Im$ is the imaginary part of a complex variable. The dislocation dipole is an infinitesimal segment $(\mathrm{d}\eta_1, \mathrm{d}\eta_2)$ of length $\mathrm{d}s$ over which a displacement jump is prescribed. For a dislocation dipole at (η_1, η_2) in x_k direction, the resulting displacement component in x_j direction at (x_1, x_2) is given by

$$G^{(\mathrm{d})}_{jk}(x_1, x_2; \eta_1, \eta_2)\,\mathrm{d}s = -\Im \frac{1}{\pi} \sum_{\alpha=1}^{3} A_{j\alpha}L_{k\alpha} \frac{\mathrm{d}\xi_\alpha}{z_\alpha - \xi_\alpha}, \tag{13}$$

where $\mathrm{d}\xi_\alpha = \mathrm{d}\eta_1 + p_\alpha \mathrm{d}\eta_2$. The detailed derivation of these solutions are given by Denda (2001).

The original boundary is discretized and approximated by a set of straight lines. The boundary displacement and traction are interpolated by the quadratic function. Since all the boundary integrals are evaluated analytically the resulting boundary equations are algebraic rather than integral equations. There is no need to deal with the singular and the hypersingular integrals. The explicit formulas for the displacement, displacement gradient, stress and the traction for generalized plane strain can be found in Denda (1999, 2001). Otherwise we follow the standard procedure of the direct BEM implementation as discussed by Denda (2001).

4. Crack modeling

4.1. Regular crack element

A crack C with the crack opening displacement δ_k of a traction-free crack in an infinite body is represented by the continuous distribution of the dislocation dipoles with the magnitude δ_k (Denda, 2001). The displacement due to the crack is given by multiplying δ_k to the fundamental dislocation dipole solution (13) and integrating over C to get

$$u_j^{(\mathrm{d})}(x_1,x_2) = -\Im\frac{1}{\pi}\int_C \sum_{\alpha=1}^{3} A_{j\alpha}\sum_{k=1}^{3} L_{k\alpha}\delta_k \frac{\mathrm{d}\xi_\alpha}{z_\alpha-\xi_\alpha}, \tag{14}$$

where $\xi_\alpha = \eta_1 + p_\alpha\eta_2$. Similarly, we can get the stress function

$$\phi_j^{(\mathrm{d})}(x_1,x_2) = -\Im\frac{1}{\pi}\int_C \sum_{\alpha=1}^{3} L_{j\alpha}\sum_{k=1}^{3} L_{k\alpha}\delta_k \frac{\mathrm{d}\xi_\alpha}{z_\alpha-\xi_\alpha}. \tag{15}$$

We approximate the curvilinear crack C by a collection of straight crack elements C_λ

$$C = \sum_{\lambda=1}^{N} C_\lambda. \tag{16}$$

If we interpolate the crack opening displacement for each crack element C_λ by the quadratic polynomial we can evaluate the integrals (14) and (15) for each element analytically (Denda, 1999, 2001). Since no crack tip singularity is built in, this crack element is called the regular crack element (RGCE). The use of the RGCEs requires the fine near crack tip mesh along the crack to simulate the high crack opening displacement gradient there. To determine the crack opening displacement δ_k, we use the traction formula and set the traction zero on one of the crack surfaces. This system of traction boundary equations will be coupled with another system of boundary equations if the the finite non-crack boundary is present and yet another system of traction boundary equations in the presence of multiple cracks. Since the crack tip singularity is not built into the interpolation, the post processing, such as the use of conservation integrals, is required to determine the stress intensity factors as demonstrated by Denda (1999, 2001). In the following sections we present alternative techniques for crack modeling using the whole crack singular elements and the crack tip singular element, each of which models the crack tip singularity analytically and provides the analytical formula for the stress intensity factors.

4.2. Whole crack singular element

Let C be a straight crack in an infinite body subject to the traction t^+ and $t^-(=-t^+)$ on its faces. It is located in the interval $(-1,+1)$ of the horizontal coordinate axis, where $\xi_\alpha = \eta_1$ for all values of $\alpha\,(=1,2,3)$ because $\eta_2 = 0$. Eqs. (14) and (15) can be written as

$$\begin{aligned} u_j^{(\mathrm{d})}(x_1,x_2) &= \Im\frac{1}{\pi}\int_{-1}^{+1} \sum_{\alpha=1}^{3} A_{j\alpha}\sum_{k=1}^{3} L_{k\alpha}\delta_k(\eta_1)\frac{\mathrm{d}\eta}{\eta_1-z_\alpha},\\ \phi_j^{(\mathrm{d})}(x_1,x_2) &= \Im\frac{1}{\pi}\int_{-1}^{+1} \sum_{\alpha=1}^{3} L_{j\alpha}\sum_{k=1}^{3} L_{k\alpha}\delta_k(\eta_1)\frac{\mathrm{d}\eta}{\eta_1-z_\alpha}. \end{aligned} \tag{17}$$

To embed the $\sqrt{r}$ crack opening displacement behavior at each crack tip we introduce the interpolation

$$\delta_k(\eta_1) = \sqrt{1-\eta_1^2}\sum_{m=1}^{M}\delta_k^{(m)}U_{m-1}(\eta_1), \tag{18}$$

where $U_{m-1}(\eta_1)$ is Chebyshev polynomial of the second kind and M is the number of polynomials. Substitute (18) into (17) and evaluate the integrals analytically to get

$$u_j^{(\mathrm{d})}(x_1,x_2) = -\Im\sum_{m=1}^{M}\sum_{\alpha=1}^{3}A_{j\alpha}\sum_{k=1}^{3}L_{k\alpha}\delta_k^{(m)}R_m(z_\alpha),$$
$$\phi_j^{(\mathrm{d})}(x_1,x_2) = -\Im\sum_{m=1}^{M}\sum_{\alpha=1}^{3}L_{j\alpha}\sum_{k=1}^{3}L_{k\alpha}\delta_k^{(m)}R_m(z_\alpha), \tag{19}$$

where

$$R_m(z_\alpha) = \left(z_\alpha - \sqrt{(z_\alpha)^2-1}\right)^m \quad (m \geqslant 1). \tag{20}$$

For the crack with half-crack length a, the interpolation and the results are still given by (18)–(20) if we replace η_1 with $E_1 = \eta_1/a$ and z_α with $Z_\alpha = z_\alpha/a$, respectively. The corresponding stress components are obtained by substituting (19), with the argument Z_α, into (11) with the result

$$\sigma_{2j}^{(\mathrm{d})}(x_1,x_2) = -\frac{1}{a}\Im\sum_{m=1}^{M}\sum_{\alpha=1}^{3}L_{j\alpha}\sum_{k=1}^{3}L_{k\alpha}\delta_k^{(m)}mG_{m-1}(Z_\alpha),$$
$$\sigma_{1j}^{(\mathrm{d})}(x_1,x_2) = \frac{1}{a}\Im\sum_{m=1}^{M}\sum_{\alpha=1}^{3}p_\alpha L_{j\alpha}\sum_{k=1}^{3}L_{k\alpha}\delta_k^{(m)}mG_{m-1}(Z_\alpha), \tag{21}$$

where

$$G^{(m-1)}(Z_\alpha) = -\frac{\left(Z_\alpha - \sqrt{(Z_\alpha)^2-1}\right)^m}{\sqrt{(Z_\alpha)^2-1}} \quad (m \geqslant 1). \tag{22}$$

The limiting value of the traction on the crack line is given by

$$(t_j)^{\pm}(X_1) = \pm\frac{1}{a}\Im\sum_{m=1}^{M}\sum_{\alpha=1}^{3}L_{j\alpha}\sum_{k=1}^{3}L_{k\alpha}\delta_k^{(m)}mU_{m-1}(X_1) \quad (|X_1| \leqslant 1), \tag{23}$$

where $X_1 = x_1/a$ and the superscripts + and − indicate limits from above and below the horizontal coordinate axis, respectively. From the limiting value of the stress on the crack line in front of each crack tip at $X_1 = \pm 1$ we get the stress intensity factors

$$K_j(\pm 1) = \sqrt{\frac{\pi}{a}}\Im\sum_{m=1}^{M}(\pm)^{m+1}m\sum_{\alpha=1}^{3}L_{j\alpha}\sum_{k=1}^{3}L_{k\alpha}\delta_k^{(m)}, \tag{24}$$

where $K_2 = K_{\mathrm{I}}$ (Mode I), $K_1 = K_{\mathrm{II}}$ (Mode II) and $K_3 = K_{\mathrm{III}}$ (Mode III). Note that (23) is the formula used to determine the crack opening displacement by setting the left-hand side to the known traction value. Once the COD is determined formula (24) can be used to calculate the SIFs.

When multiple straight center cracks are present in the infinite body we introduce the local coordinate system for each crack such that the crack is centered at the origin and aligned with the horizontal axis. The formulas (17)–(24) still apply if we calculate the compliance tensor, characteristic roots, and matrices **L** and **A** in the local rotated coordinate system. The local components obtained by these formulas must be transformed to the global component before they are added to the contributions from other cracks. When the finite boundary is present the coupling of the boundary equations and the crack surface traction equations present the overall system of equations to be solved for the unknown boundary displacement/traction and the crack opening displacement. The results of crack analysis for multiple straight cracks have been reported by Denda and Mattingly (2003).

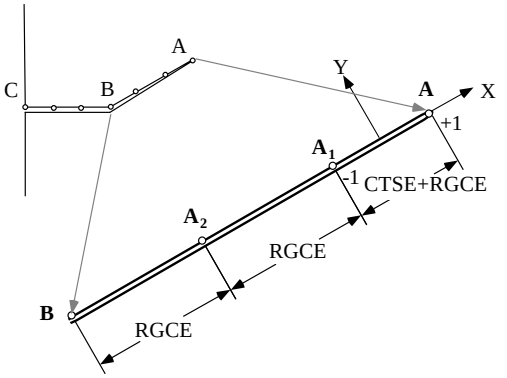

Fig. 1. Crack tip singular element (CTSE) AA_1 superposed on the regular crack elements (RGCEs).

4.3. Crack tip singular element

We extend the use of the WCSE, which is limited so far to straight center cracks, to curvilinear and/or edge cracks. Discretize the original curvilinear crack into a collection of multiple straight crack elements as shown in Fig. 1; the crack opening displacement in each element is interpolated by the quadratic polynomial. This is the regular crack element scheme introduced earlier, which is a complete scheme by itself but lacks the ability to model the crack tip singularity analytically. So we modify the crack tip element AA_1 (Fig. 1) by superposing the whole crack singular element $AA_1^{(s)}$ on top of the existing regular crack tip element $AA_1^{(r)}$ to embed the correct singular behavior at the crack tip A. The size of the WCSE $AA_1^{(s)}$ is selected small enough (compared to the crack length) so that only one term of the interpolation (18) is sufficient. The WCSE used at the crack tip with only one term of interpolation is called the crack tip singular element (CTSE). A center crack has two CTSEs, while an edge crack has one. A set of simple formulas for the CTSE, obtained by setting $M = 1$ in the results of the WCSE, is summarized below. Introduce the local coordinate system (x_1, x_2) with the origin at the center of the CTSE. The generalized complex variables are defined by $z_\alpha = x_1 + p_\alpha x_2$, where p_α ($\alpha = 1, 2, 3$) are the characteristic roots in the local coordinate system. The CTSE is located in the interval $(-a, +a)$ along the x_1-axis whose positive direction points toward the crack tip as shown in Fig. 1. The crack opening displacement is interpolated by

$$\delta_k(X_1) = \sqrt{1 - X_1^2}\,\delta_k^{(1)}, \tag{25}$$

where $X_1 = x_1/a$. The displacement and the stress function contribution are given by

$$\begin{aligned} u_j^{(d)}(x_1, x_2) &= -\Im \sum_{\alpha=1}^{3} A_{j\alpha} \sum_{k=1}^{3} L_{k\alpha}\delta_k^{(1)} R_1(Z_\alpha), \\ \phi_j^{(d)}(x_1, x_2) &= -\Im \sum_{\alpha=1}^{3} L_{j\alpha} \sum_{k=1}^{3} L_{k\alpha}\delta_k^{(1)} R_1(Z_\alpha), \end{aligned} \tag{26}$$

where

$$R_1(Z_\alpha) = Z_\alpha - \sqrt{(Z_\alpha)^2 - 1}, \tag{27}$$

and $Z_\alpha = z_\alpha/a$. The limiting value of the traction on the crack line is given by

$$(t_j)^{\pm}(X_1) = \pm\frac{1}{a}\Im \sum_{\alpha=1}^{3} L_{j\alpha} \sum_{k=1}^{3} L_{k\alpha}\delta_k^{(1)} \quad (|X_1| \leqslant 1) \tag{28}$$

and the stress intensity factors by

$$K_j(+1) = \sqrt{\frac{\pi}{a}}\Im \sum_{\alpha=1}^{3} L_{j\alpha} \sum_{k=1}^{3} L_{k\alpha}\delta_k^{(1)}, \tag{29}$$

where $K_2 = K_{\mathrm{I}}$ (Mode I), $K_1 = K_{\mathrm{II}}$ (Mode II) and $K_3 = K_{\mathrm{III}}$ (Mode III).

Note that the CTSE provides the $1/\sqrt{r}$ stress singularity at its two ends A and A_1 in Fig. 1. While the singularity at A reflect the true crack tip singular behavior, the singularity at A_1 is spurious, i.e., within the element the stress varies like $1/\sqrt{\rho}$ near A_1, where ρ is the distance from A_1. Note also the stress contribution from the superimposed regular element $AA_1^{(\mathrm{r})}$ varies like $1/\rho$ near A_1, which is stronger singularity than the spurious $1/\sqrt{\rho}$ singularity. Thus if we select the collocation point of the regular crack element $AA_1^{(\mathrm{r})}$ off a small distance ρ away from A_1, the effect of the spurious $1/\sqrt{\rho}$ singularity at A_1 is overwhelmed by that of stronger $1/\rho$ singularity. Since such a selection of the collocation point is the standard procedure of the discontinuous element, we can justify the use of the CTSE. The suggested offset distance for the discontinuous element is between 1/40 and 1/20 of the element size. Extension of the above results to multiple curvilinear cracks in the presence of the finite boundary requires the consideration of the coupling among cracks and the boundary, which is performed in a straightforward fashion.

5. Numerical results

The crack opening displacement is modelled by the regular crack elements (RGCEs) over the entire crack segment first. Additional accuracy is provided by further introducing the crack tip singular element (CTSE) for each crack tip element. The accuracy of the numerical results depends both on the CTSE and the selection of the regular crack elements. Denda (1999, 2001) used the regular crack elements to model curvilinear cracks in the main processing and determined the SIFs using the conservation integral of Chen and Shield (1977) in the post processing. The remarkable accuracy of the SIF results by Denda (1999, 2001) is a testimony of the reliability of the regular crack element; even without using the CTSE the numerical results are quite accurate. However, the post processing evaluation of the conservation integrals is required to get the stress intensity factors. The CTSE eliminates this post processing requirement. In the following the results by the CTSE will be compared primarily with those by the RGCE with the conservation integral to demonstrate the accuracy of the CTSE.

Several crack element meshes for a center (in an infinite body) and an edge crack (in a semi-infinite body) under uniaxial tension are studied for isotropic solids. The degenerate (or coincident) characteristic roots of the isotropic material are made distinct by slightly perturbing the compliance coefficients. Fig. 2 shows typical crack element meshes for a center crack of length $2a$, where c is the crack tip element size. Fig. 3

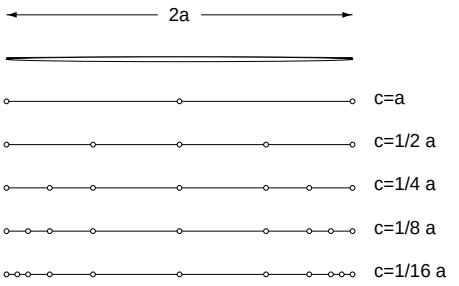

Fig. 2. Symmetric crack elements for a center crack.

shows two sets of symmetrical and asymmetrical crack elements for an edge crack of length a. The asymmetrical element recognizes the absence of singularity at the crack mouth and adopts the arrangement used for one half of the center crack. The results are summarized in Tables 1 and 2 and compared with those obtained by the isotropic CTSE of Denda and Dong (1997). The agreement is near perfect between the two sets of results giving the confidence on the new CTSE for anisotropic solids. The recommendation based on this study is to use the symmetric mesh with $c = 1/16a$ (Fig. 2) for the center crack and the asymmetric mesh with $c = 1/16a$ (Fig. 3(b)) for the edge crack. If we define the near crack tip segment to be one half of a straight center crack or the whole of a straight edge crack, then the recommendation is to select c to be 1/16 of the near crack tip segment length. Unless mentioned otherwise, we will use these meshes below.

In the following examples, we select aluminum crystal (cubic) as the model anisotropic solid. Originally the crystal axes a_1, a_2 and a_3 of the cubic lattice are aligned along the coordinate axes x_1, x_2 and x_3. Then we rotate the axes three times: θ, ψ and ϕ. First rotate the coordinate system through an angle θ about the x_3-axis, then an angle ψ about the rotated x_2-axis, and finally an angle ϕ about the rotated x_3-axis. Four compliance matrices produced this way are given by

$$\mathbf{s}_{[0,0,0]} = \begin{bmatrix} s_{11} & s_{12} & s_{13} & s_{14} & s_{15} & s_{16} \\ & s_{22} & s_{23} & s_{24} & s_{25} & s_{26} \\ & & s_{33} & s_{34} & s_{35} & s_{36} \\ & & & s_{44} & s_{45} & s_{46} \\ & & & & s_{55} & s_{56} \\ & & & & & s_{66} \end{bmatrix} = \begin{bmatrix} 15.9 & -5.8 & -5.8 & 0 & 0 & 0 \\ & 15.9 & -5.8 & 0 & 0 & 0 \\ & & 15.9 & 0 & 0 & 0 \\ & & & 35.2 & 0 & 0 \\ & & & & 35.2 & 0 \\ & & & & & 35.2 \end{bmatrix}, \tag{30}$$

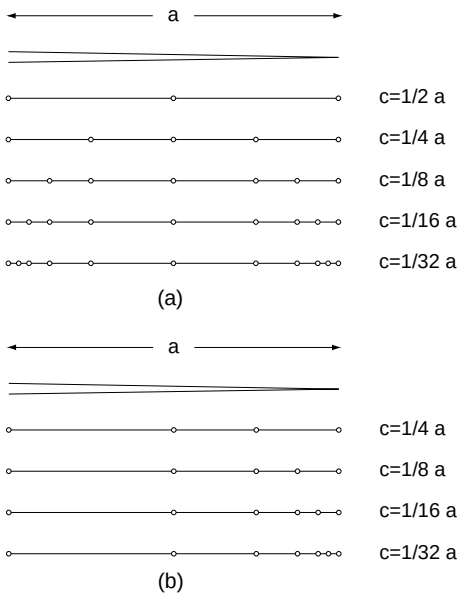

Fig. 3. (a) Symmetric and (b) asymmetric crack elements for an edge crack.

Table 1
The effect of crack tip singular element size on the stress intensity factor K_I/K_I^{anal} of a center crack (Fig. 2) in an infinite isotropic plate under uniaxial tension, where K_I^{anal} is the analytical solution

$c = a$	1.010(1.010)
$c = a/2$	1.006(1.006)
$c = a/4$	1.003(1.003)
$c = a/8$	1.001(1.001)
$c = a/16$	1.000(1.000)
$c = a/32$	0.999(0.999)
$c = a/64$	0.999(0.999)

The values in the parentheses are obtained by the isotropic CTSE (Denda and Dong, 1999).

Table 2
The effect of crack tip singular element size on the stress intensity factor K_I/K_I^{anal} of an edge crack (Fig. 3) in a semi-infinite isotropic plate under uniaxial tension σ, where $K_I^{anal} = 1.12\sigma\sqrt{\pi a}$ is the analytical solution

	Symmetrical mesh	Asymmetrical mesh
	K_I/K_I^{anal}	K_I/K_I^{anal}
$c = a/2$	1.011(1.010)	1.011(1.010)
$c = a/4$	1.006(1.006)	1.006(1.007)
$c = a/8$	1.004(1.004)	1.004(1.004)
$c = a/16$	1.002(1.002)	1.003(1.003)
$c = a/32$	1.001(1.001)	1.002(1.002)
$c = a/64$	1.000(1.000)	1.002(1.002)
$c = a/128$	1.000(1.000)	1.001(1.001)
$c = a/256$	0.999(0.999)	1.001(1.001)

The values in the parentheses are obtained by the isotropic CTSE (Denda and Dong, 1999).

$$\mathbf{s}_{[30,0,0]} = \begin{bmatrix} 14.362 & -4.2625 & -5.8 & 0 & 0 & -1.7754 \\ & 14.362 & -5.8 & 0 & 0 & 1.7754 \\ & & 15.9 & 0 & 0 & 0 \\ & & & 35.2 & 0 & 0 \\ & & & & 35.2 & 0 \\ & & & & & 41.35 \end{bmatrix}, \tag{31}$$

$$\mathbf{s}_{\left[45,\arccos\frac{1}{\sqrt{3}},0\right]} = \begin{bmatrix} 13.85 & -5.1167 & -4.4333 & 0 & -1.9328 & 0 \\ & 13.85 & -4.4333 & 0 & 1.9328 & 0 \\ & & 13.167 & 0 & 0 & 0 \\ & & & 40.667 & 0 & 3.8655 \\ & & & & 40.667 & 0 \\ & & & & & 37.933 \end{bmatrix}, \tag{32}$$

$$\mathbf{s}_{\left[45,\arccos\frac{1}{\sqrt{3}},45\right]} = \begin{bmatrix} 13.85 & -5.1167 & -4.4333 & 1.3667 & 1.3667 & 0 \\ & 13.85 & -4.4333 & -1.3667 & -1.3667 & 0 \\ & & 13.167 & 0 & 0 & 0 \\ & & & 40.667 & 0 & -2.7333 \\ & & & & 40.667 & 2.7333 \\ & & & & & 37.933 \end{bmatrix}, \tag{33}$$

in units of 10^{-12} m^2/N showing only the upper halves of the symmetric matrices. Three numbers in $\mathbf{s}_{[\theta,\psi,\phi]}$ indicate the three rotation angles θ, ψ and ϕ in degrees. Notice that each crack configuration considered is not rotated even though rotations are used to produce different compliance matrices.

For two (Fig. 4 with $2a/d = 0.9$) and three (Fig. 5 with $2a/d = 0.9$) collinear cracks in an infinite body subject to the single mode tension loading, three modes are decoupled and the stress intensity factors are independent on the elastic constants of the solid (Denda, 2001). The values of K_{I} under the uniaxial tension is listed in Tables 3 (two collinear cracks) and 4 (three collinear cracks) for four compliance matrices (30)–(33) and compared with the results by the RGCE (Denda, 2001) and the stress intensity handbook (Murakami et al., 1987). Values of K_{II} and K_{III}, not listed in the tables, are zero up to the fourth decimal point (i.e., 0.0000). The accuracy of the handbook (Murakami et al., 1987) value for the two collinear cracks is 0.5% and the discrepancy between the handbook and the CTSE values is less than 0.5%.

Stress intensity factors for two aligned parallel cracks (Fig. 6 with $2a/d = 5.0$), three aligned parallel cracks (Fig. 7 with $2a/d = 0.8$), and two inclined cracks (Fig. 8 with $\alpha = 30°$ and $2a/d = 0.9$) subject to

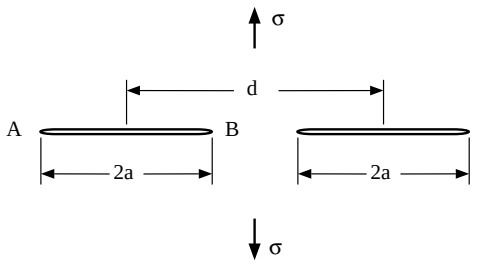

Fig. 4. Two collinear cracks under remote uniaxial tension.

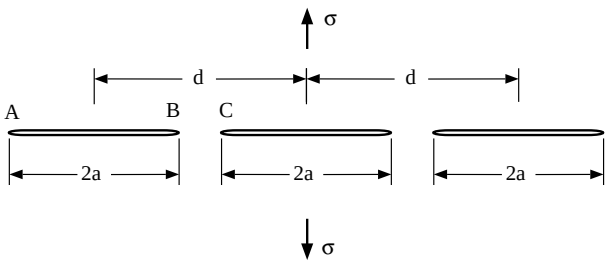

Fig. 5. Three collinear cracks under remote uniaxial tension.

Table 3
Stress intensity factors for two collinear cracks (Fig. 4 with $2a/d = 0.9$) in an infinite body under tension σ

	$\mathbf{s}_{[0,0,0]}$	$\mathbf{s}_{[30,0,0]}$	$\mathbf{s}_{\left[45,\arccos 1/\sqrt{3},0\right]}$	$\mathbf{s}_{\left[45,\arccos 1/\sqrt{3},45\right]}$	Handbook
$K_{\mathrm{IA}}/\sigma\sqrt{\pi a}$	1.118(1.117)	1.118(1.117)	1.118(1.117)	1.118(1.117)	1.117
$K_{\mathrm{IB}}/\sigma\sqrt{\pi a}$	1.458(1.450)	1.458(1.450)	1.458(1.450)	1.458(1.450)	1.454

The values in the parentheses are taken from Denda (2001). Handbook values by Murakami et al. (1987).

Table 4
Stress intensity factors for three collinear cracks (Fig. 5 with $2a/d = 0.9$) in an infinite body under tension σ

	$\mathbf{s}_{[0,0,0]}$	$\mathbf{s}_{[30,0,0]}$	$\mathbf{s}_{[45,\arccos 1/\sqrt{3},0]}$	$\mathbf{s}_{[45,\arccos 1/\sqrt{3},45]}$	Handbook
$K_{IA}/\sigma\sqrt{\pi a}$	1.166(1.163)	1.165(1.163)	1.166(1.163)	1.166(1.163)	1.164
$K_{IB}/\sigma\sqrt{\pi a}$	1.570(1.559)	1.569(1.559)	1.570(1.559)	1.570(1.559)	1.565
$K_{IC}/\sigma\sqrt{\pi a}$	1.612(1.601)	1.612(1.601)	1.612(1.601)	1.612(1.601)	1.607

The values in the parentheses are taken from Denda (2001). Handbook values by Murakami et al. (1987).

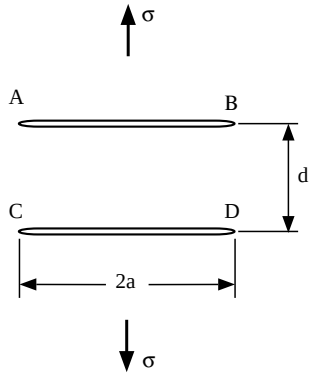

Fig. 6. Two aligned parallel cracks under remote uniaxial tension.

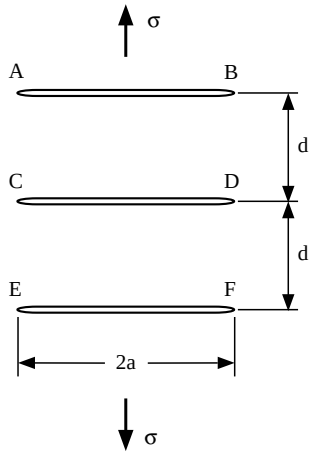

Fig. 7. Three aligned parallel cracks under remote uniaxial tension.

the uniaxial tension are given in Tables 5–7 in comparison with those by the RGCE (Denda, 2001). The SIF results of these crack configurations depend on the elastic constants. Two parallel edge cracks in a half-plane subject to the uniaxial tension is shown in Fig. 9. Numerical results for the stress intensity factors along with those by the RGCE (Denda, 2001) are given in Table 8. A kinked crack in a half-plane

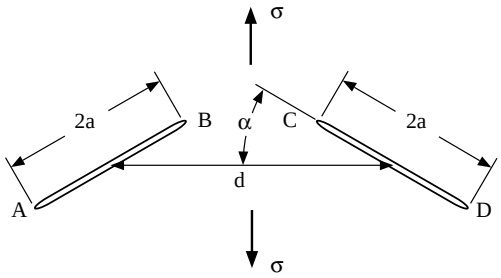

Fig. 8. Two inclined cracks under remote uniaxial tension.

Table 5
Stress intensity factors for aligned two parallel cracks (Fig. 6 with $2a/d = 5.0$) in an infinite body under tension σ

		$\mathbf{s}_{[0,0,0]}$	$\mathbf{s}_{[30,0,0]}$	$\mathbf{s}_{[45,\arccos 1/\sqrt{3},0]}$	$\mathbf{s}_{[45,\arccos 1/\sqrt{3},45]}$
$K_{\mathrm{I}}/\sigma\sqrt{\pi a}$	A	0.721(0.722)	0.708(0.712)	0.721(0.723)	0.721(0.723)
	B	0.721(0.722)	0.734(0.734)	0.721(0.723)	0.720(0.722)
	C	0.721(0.722)	0.734(0.734)	0.721(0.723)	0.720(0.722)
	D	0.721(0.722)	0.708(0.712)	0.721(0.723)	0.721(0.723)
$K_{\mathrm{II}}/\sigma\sqrt{\pi a}$	A	0.170(0.171)	0.159(0.162)	0.164(0.164)	0.163(0.164)
	B	−0.170(−0.171)	−0.161(−0.158)	−0.164(−0.164)	−0.163(−0.164)
	C	−0.170(−0.171)	−0.161(−0.158)	−0.164(−0.164)	−0.163(−0.164)
	D	0.170(0.171)	0.159(0.162)	0.164(0.164)	0.163(0.164)
$K_{\mathrm{III}}/\sigma\sqrt{\pi a}$	A	0.000(0.000)	0.000(0.000)	0.012(0.012)	−0.008(−0.008)
	B	0.000(0.000)	0.000(0.000)	0.012(0.012)	−0.010(−0.010)
	C	0.000(0.000)	0.000(0.000)	−0.012(−0.012)	0.010(0.010)
	D	0.000(0.000)	0.000(0.000)	−0.012(−0.012)	0.008(0.008)

The values in the parentheses are taken from Denda (2001).

under uniaxial tension is shown in Fig. 10. The non-crack boundary of the semi-infinite body is modeled by 34 elements consisting of a gradually refined mesh as the crack mouth is approached. We have used twelve crack elements (6 for each of the straight segments) along the kinked crack; the size of the singular crack tip element is 1/8 of the near crack tip segment. The numerical results for the SIFs are given in Table 9 along with the analytical solution for the isotropic solids given in the stress intensity handbook (Murakami et al., 1987). The SIFs for double edge cracks in a square plate, as shown in Fig. 11, are given for the isotropic solid and the cubic aluminum crystal $\mathbf{s}_{[0,0,0]}$ in Table 10 along with the isotropic solution by Bowie (1964). Exploiting the symmetry of the problem only one half of the plate was analyzed. For the crack tip singular element, the size of the crack tip element is $c = a/32$ with the asymmetric arrangement of the crack elements shown in Fig. 3(b). The accuracy of the Bowie solution is unknown. In summary, the typical discrepancy between the SIF results by the CTSE and the RGCE with the conservation integral, for all the problems tested above, is 0.25%. This excellent agreement provides a great confidence in the accuracy of the proposed CTSE, which is faster than the latter due to the absence of the post-processing requirement.

Table 6
Stress intensity factors for aligned three parallel cracks (Fig. 7 with $2a/d = 0.8$) in an infinite body under tension σ

		$\mathbf{s}_{[0,0,0]}$	$\mathbf{s}_{[30,0,0]}$	$\mathbf{s}_{[45,\arccos 1/\sqrt{3},0]}$	$\mathbf{s}_{[45,\arccos 1/\sqrt{3},45]}$
$K_{\mathrm{I}}/\sigma\sqrt{\pi a}$	A	0.861(0.861)	0.831(0.832)	0.849(0.850)	0.850(0.850)
	B	0.861(0.861)	0.856(0.856)	0.849(0.850)	0.848(0.849)
	C	0.768(0.769)	0.742(0.743)	0.751(0.752)	0.751(0.752)
	D	0.768(0.769)	0.742(0.743)	0.751(0.752)	0.751(0.752)
	E	0.861(0.861)	0.856(0.856)	0.849(0.850)	0.848(0.849)
	F	0.861(0.861)	0.831(0.832)	0.849(0.850)	0.850(0.850)
$K_{\mathrm{II}}/\sigma\sqrt{\pi a}$	A	0.043(0.043)	0.042(0.046)	0.045(0.045)	0.044(0.044)
	B	−0.043(−0.043)	−0.049(−0.045)	−0.045(−0.045)	−0.045(−0.045)
	C	0.000(0.000)	−0.0013(0.0025)	0.000(0.000)	−0.00036(−0.00036)
	D	0.000(0.000)	−0.0013(0.0025)	0.000(0.000)	−0.00036(−0.00036)
	E	−0.043(−0.043)	−0.049(−0.045)	−0.045(−0.045)	−0.045(−0.045)
	F	0.043(0.043)	0.042(0.046)	0.045(0.045)	0.044(0.044)
$K_{\mathrm{III}}/\sigma\sqrt{\pi a}$	A	0.000(0.000)	0.000(0.000)	0.0066(0.0066)	0.0015(0.0015)
	B	0.000(0.000)	0.000(0.000)	0.0066(0.0066)	−0.011(−0.011)
	C	0.000(0.000)	0.000(0.000)	0.000(0.000)	0.0098(0.0097)
	D	0.000(0.000)	0.000(0.000)	0.000(0.000)	−0.0098(−0.0097)
	E	0.000(0.000)	0.000(0.000)	−0.0066(−0.0066)	0.011(0.011)
	F	0.000(0.000)	0.000(0.000)	−0.0066(−0.0066)	−0.0015(−0.0015)

The values in the parentheses are taken from Denda (2001).

Table 7
Stress intensity factors for two inclined cracks (Fig. 8 with $\alpha = 30°$ and $2a/d = 0.9$) in an infinite body under tension σ

		$\mathbf{s}_{[0,0,0]}$	$\mathbf{s}_{[30,0,0]}$	$\mathbf{s}_{[45,\arccos 1/\sqrt{3},0]}$	$\mathbf{s}_{[45,\arccos 1/\sqrt{3},45]}$
$K_{\mathrm{I}}/\sigma\sqrt{\pi a}$	A	0.788(0.788)	0.792(0.788)	0.788(0.788)	0.788(0.788)
	B	0.911(0.909)	0.918(0.913)	0.914(0.911)	0.913(0.911)
	C	0.912(0.909)	0.910(0.912)	0.914(0.911)	0.914(0.911)
	D	0.788(0.788)	0.785(0.788)	0.788(0.788)	0.788(0.788)
$K_{\mathrm{II}}/\sigma\sqrt{\pi a}$	A	0.474(0.474)	0.472(0.474)	0.475(0.475)	0.475(0.475)
	B	0.455(0.454)	0.451(0.452)	0.455(0.454)	0.455(0.454)
	C	−0.455(−0.454)	−0.458(−0.454)	−0.455(−0.454)	−0.454(−0.454)
	D	−0.474(−0.474)	−0.478(−0.476)	−0.475(−0.475)	−0.475(−0.475)
$K_{\mathrm{III}}/\sigma\sqrt{\pi a}$	A	0.000(0.000)	0.000(0.000)	−0.00036(−0.00036)	−0.00032(−0.00032)
	B	0.000(0.000)	0.000(0.000)	−0.001(−0.001)	0.002(0.002)
	C	0.000(0.000)	0.000(0.000)	−0.001(−0.001)	−0.00041(−0.00039)
	D	0.000(0.000)	0.000(0.000)	−0.00036(−0.00036)	0.001(0.001)

The values in the parentheses are taken from Denda (2001).

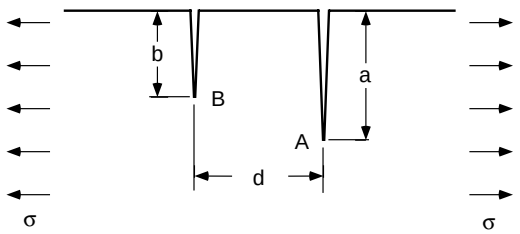

Fig. 9. Two parallel edge cracks in a half-plane under remote uniaxial tension.

Table 8
Stress intensity factors for two parallel edge cracks (Fig. 9) in a half-plane in tension σ

		$\mathbf{s}_{[0,0,0]}$	$\mathbf{s}_{[30,0,0]}$	$\mathbf{s}_{[45,\arccos 1/\sqrt{3},0]}$	$\mathbf{s}_{[45,\arccos 1/\sqrt{3},45]}$
$K_{\mathrm{I}}/\sigma\sqrt{\pi a}$	A	0.870(0.870)	0.860(0.860)	0.859(0.859)	0.858(0.858)
	B	0.870(0.870)	0.845(0.846)	0.859(0.859)	0.859(0.859)
$K_{\mathrm{II}}/\sigma\sqrt{\pi a}$	A	−0.138(−0.138)	−0.133(−0.133)	−0.133(−0.133)	−0.133(−0.133)
	B	0.138(0.138)	0.128(0.128)	0.133(0.133)	0.132(0.132)
$K_{\mathrm{III}}/\sigma\sqrt{\pi a}$	A	0.000(0.000)	0.000(0.000)	0.007(0.007)	−0.012(−0.012)
	B	0.000(0.000)	0.000(0.000)	−0.007(−0.007)	−0.002(−0.002)

The values in the parentheses are taken from Denda (2001).

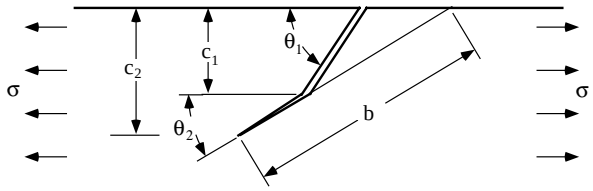

Fig. 10. A kinked edge crack in a half-plane under remote uniaxial tension.

Table 9
Stress intensity factors for a kinked edge crack (Fig. 10 with $\theta_1 = 90°$, $\theta_2 = 45°$ and $c_2 = 1.0$) in a half-plane under tension

c_1	Isotropic	Handbook	$\mathbf{s}_{[0,0,0]}$	$\mathbf{s}_{[30,0,0]}$	$\mathbf{s}_{[45,\arccos 1/\sqrt{3},0]}$	$\mathbf{s}_{[45,\arccos 1/\sqrt{3},45]}$
$K_{\mathrm{I}}/\sigma\sqrt{\pi b}$						
0.25	0.706(0.706)	0.703	0.717	0.701	0.707	0.707
0.50	0.706(0.706)	0.704	0.717	0.701	0.706	0.706
0.75	0.704(0.706)	0.705	0.716	0.698	0.705	0.705
0.90	0.705(0.706)	0.707	0.717	0.699	0.706	0.706
$K_{\mathrm{II}}/\sigma\sqrt{\pi b}$						
0.25	−0.366(−0.365)	−0.365	−0.363	−0.367	−0.367	−0.366
0.50	−0.367(−0.365)	−0.365	−0.363	−0.368	−0.367	−0.367
0.75	−0.367(−0.366)	−0.366	−0.363	−0.368	−0.368	−0.367
0.90	−0.360(−0.359)	−0.359	−0.355	−0.361	−0.360	−0.359

The values in the parentheses are taken from Denda and Dong (1999). Handbook values by Murakami et al. (1987).

6. Concluding remarks

We have developed a singular crack tip element (SCTE) for the general anisotropic solids with the built in $\sqrt{r}$ displacement and $1/\sqrt{r}$ singular stress behaviors at its tip, which is placed at each tip of each crack. The number and the shape of the crack that can be model by the technique are unlimited. Over the crack tip element of small length $2a$ we interpolate the crack opening displacement by

$$\delta_k(X_1) = \sqrt{1 - X_1^2}\,\delta_k^{(1)}$$

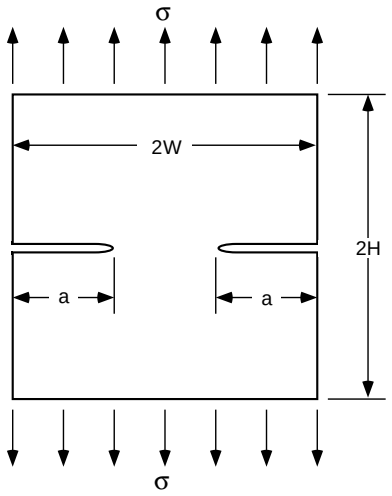

Fig. 11. Double edge cracks in a square plate ($W = H$) in tension.

Table 10
Stress intensity factors for double edge cracks in a square plate ($H/W = 1$) under tension (Fig. 11), where $\eta(a/W, H/W) = K_I/\{\sigma\sqrt{2W\tan(\pi a/2W)}\}$

a/W	$\eta(a/W, H/W)$		
	Isotropic	Bowie (1964)	$\mathbf{s}_{[0,0,0]}$
0.1	1.13(1.13)	1.13	1.14
0.2	1.16(1.16)	1.13	1.17
0.4	1.19(1.19)	1.16	1.20
0.8	1.05(1.05)	1.01	1.05

The values in the parentheses are taken from Denda and Dong (1999).

along the local crack axis $X_1(= x_1/a)$. The resulting displacement contribution is given by

$$u_j^{(\mathrm{d})}(x_1, x_2) = -\Im \sum_{\alpha=1}^{3} A_{j\alpha} \sum_{k=1}^{3} L_{k\alpha}\delta_k^{(1)} R_1(Z_\alpha)$$

and the stress intensity factors by

$$K_j(+1) = \sqrt{\frac{\pi}{a}}\Im \sum_{\alpha=1}^{3} L_{j\alpha} \sum_{k=1}^{3} L_{k\alpha}\delta_k^{(1)},$$

where

$$R_1(Z_\alpha) = Z_\alpha - \sqrt{(Z_\alpha)^2 - 1},$$

and $Z_\alpha = z_\alpha/a$. The stress intensity factors, along with the unknown boundary displacements and tractions, are determined in the main processing; no post processing is required. The accuracy of the stress intensity

factors is comparable to that obtained by the well established RGCE that requires the evaluation of conservation integral in the post processing.

Acknowledgements

Denda was supported by the NSF IGERT grant under a subcontract from the University of Tennessee, Knoxville. Marante acknowledges the FONACIT of Venezuela for its support to stay at Rutgers University as a visiting scholar.

References

Altiero, N.J., Gavazza, S.D., 1980. On a unified boundary-integral equation method. J. Elast. 10 (1), 1–9.
Ang, W.T., Clements, D.L., 1986. A boundary element method for determining the effect of holes on the stress distribution around a crack. Int. J. Numer. Methods Eng. 23, 1727–1737.
Berger, J.R., Tewary, V.K., 1997. Boundary integral equation formulation for interface cracks in anisotropic materials. Int. J. Numer. Methods Eng. 20, 261–266.
Bowie, O.L., 1964. Rectangular tensile sheet with symmetric edge cracks. J. Appl. Mech. 31 (2), 208–212.
Chen, F.H.K., Shield, R.T., 1977. Conservation laws in elasticity of the J-integral type. J. Appl. Math. Phys. (ZAMP) 28, 1–22.
Denda, M., 1999. A dislocation and point force approach to the boundary element method for mixed mode crack analysis of plane anisotropic solids. J. Chinese Inst. Eng. 22 (6), 677–693.
Denda, M., 2001. Mixed mode I, II and III analysis of multiple cracks in plane anisotropic solids by the BEM: a dislocation and point force approach. Int. J. Eng. Anal. Bound. Elements 25 (4–5), 267–278.
Denda, M., Dong, Y.F., 1997. Complex variable approach to the BEM for multiple crack problems. Computational Methods in Applied Mechanics and Engineering 141 (3–4), 247–264.
Denda, M., Dong, Y.F., 1999. Analytical formulas for a 2-D crack tip singular boundary element for rectilinear cracks and crack growth analysis. Int. J. Eng. Anal. Bound. Elements 23, 35–49.
Denda, M., Mattingly, E., 2003. The singular crack element for2-d boundary element analysis of multiple straight cracks in the general anisotropic solids. Electronic J. Boundary Elements 1 (3), 404–417.
Eshelby, J.D., 1969. The elastic field of a crack extending non-uniformly under general anti-plane loading. J. Mech. Phys. Solids 17, 177–199.
Eshelby, J.D., Read, W.T., Shockley, W., 1953. Anisotropic elasticity with applications to dislocation theory. Acta Metall. 1, 251–259.
Lekhnitskii, S.G., 1963. Theory of Elasticity of an Anisotropic Elastic Body. Hoden-Day, San Francisco.
Murakami, Y. et al., 1987. Stress Intensity Factor Handbook. Pergamon Press, Oxford.
Snyder, M.D., Cruse, T.A., 1975. Boundary integral equation analysis of cracked anisotropic plates. Int. J. Fract. 11, 315–328.
Sollero, P., Aliabadi, M.H., 1993. Fracture mechanics analysis of anisotropic plates by the boundary element method. Int. J. Fract. 64 (4), 269–284.
Tan, C.L., Gao, Y.L., 1992. Boundary element analysis of plane anisotropic bodies with stress concentrations and cracks. Compos. Struct. 20, 17–28.
Tan, C.L., Gao, Y.L., Afagh, F.F., 1992. Boundary element analysis of interface cracks between dissimilar anisotropic materials. Int. J. Solids Struct. 29 (24), 3201–3220.